Investigating the Mechanism of Substrate Uptake and Release in the Glutamate Transporter Homologue Glt$_{Ph}$ through Metadynamics Simulations

Giovanni Grazioso,[†] Vittorio Limongelli,[‡,§,⊥] Davide Branduardi,[#] Ettore Novellino,[⊥] Carlo De Micheli,[†] Andrea Cavalli,[*,#,△] and Michele Parrinello[*,‡,§]

[†]Dipartimento di Scienze Farmaceutiche "Pietro Pratesi", Università degli Studi di Milano, Via Mangiagalli 25, I-20133 Milano, Italy

[‡]Department of Chemistry and Applied Biosciences, Eidgenössiche Technische Hochschule (ETH), Zurich, Switzerland

[§]Institute of Computational Science (ICS), Università della Svizzera Italiana, Via Giuseppe Buffi 13, CH-6900 Lugano, Switzerland
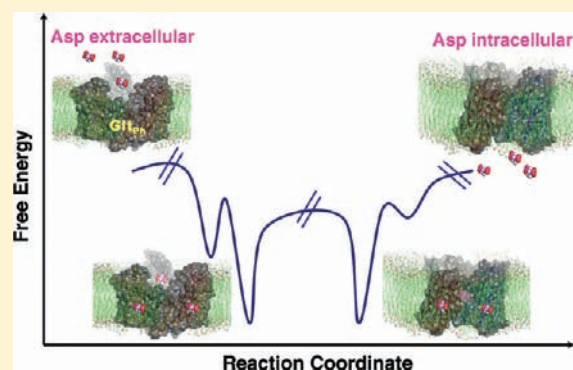
[⊥]Dipartimento di Chimica Farmaceutica e Tossicologica, Università di Napoli "Federico II", Via D. Montesano, 49, I-80131 Napoli, Italy

[#]Department of Drug Discovery and Development, Italian Institute of Technology, Via Morego 30, I-16163 Genoa, Italy

[△]Department of Pharmaceutical Sciences, University of Bologna, Via Belmeloro 6, I-40126 Bologna, Italy

S Supporting Information

ABSTRACT: A homeostatic concentration of glutamate in the synaptic cleft ensures a correct signal transduction along the neuronal network. An unbalance in this concentration can lead to neuronal death and to severe neurodegenerative diseases such as Alzheimer's or Parkinson's. Glutamate transporters play a crucial role in this respect because they are responsible for the reuptake of the neurotransmitter from the synaptic cleft, thus controlling the glutamate concentration. Understanding the molecular mechanism of this transporter can provide the possibility of an exogenous control. Structural studies have shown that this transporter can assume at least three conformations, thus suggesting a pronounced dynamical behavior. However, some intermediate states that lead to the substrate internalization have not been characterized and many aspects of the transporter mechanism still remain

unclear. Here, using metadynamics simulations, we investigate the substrate uptake from the synaptic cleft and its release in the intracellular medium. In addition, we focus on the role of ions and substrate during these processes and on the stability of the different conformations assumed by the transporter. The present dynamical results can complement available X-ray data and provide a thorough description of the entire process of substrate uptake, internalization, and release.

INTRODUCTION

The excitatory neurotransmitters, such as (S)-glutamate (Glu) and (S)-aspartate (Asp), play key roles in propagating the signal along neural pathways.[1] Under physiological conditions, the concentration of neurotransmitter in the synaptic cleft is finely regulated by specific sodium-dependent membrane proteins, known as excitatory amino acids transporters (EAATs).[2] In mammals, malfunctioning of EAATs is related to an unbalance of Glu concentration that leads to an extracellular increase of glutamate that has been associated to several neurodegenerative diseases, such as Alzheimer's or Parkinson's.[3] Therefore, the possibility of modulating the uptake mechanism represents a convenient way to control Glu concentration and hopefully the related diseases.

During recent years, a number of studies have shed light on many aspects of the molecular mechanism of glutamate transport. An important contribution comes from Yernool et al., who reported the X-ray structure of the Glu transporter from *Pyrococcus horikoshii* (Glt$_{Ph}$).[4,5] This prokaryotic form shares 36%

sequence identity with the eukaryotic form, thus representing a useful model for understanding the human EAAT functionality.[4] It has been shown that in the cell, the bowl-shaped Glt$_{Ph}$ trimer is embedded in the membrane and forms a solvent-filled basin in the extracellular region. The transport of the substrate is assisted by the cotransport of two Na$^+$ ions and is mediated by the concerted motion of the transmembrane domain 7 (TM7) and the two hairpins (HP1 and HP2) that regulate the access to either side of the membrane (Figure 1A).

Yernool et al.[4] and Reyes et al.[6] have reported that this transporter may assume at least four different conformational states, which have been classified as follows: (i) outward facing open (OFOp) where the Glu binding site is exposed toward the extracellular region and HP2 is in the open state; (ii) outward facing occluded (OFOc), with HP2 in the closed state; (iii) the
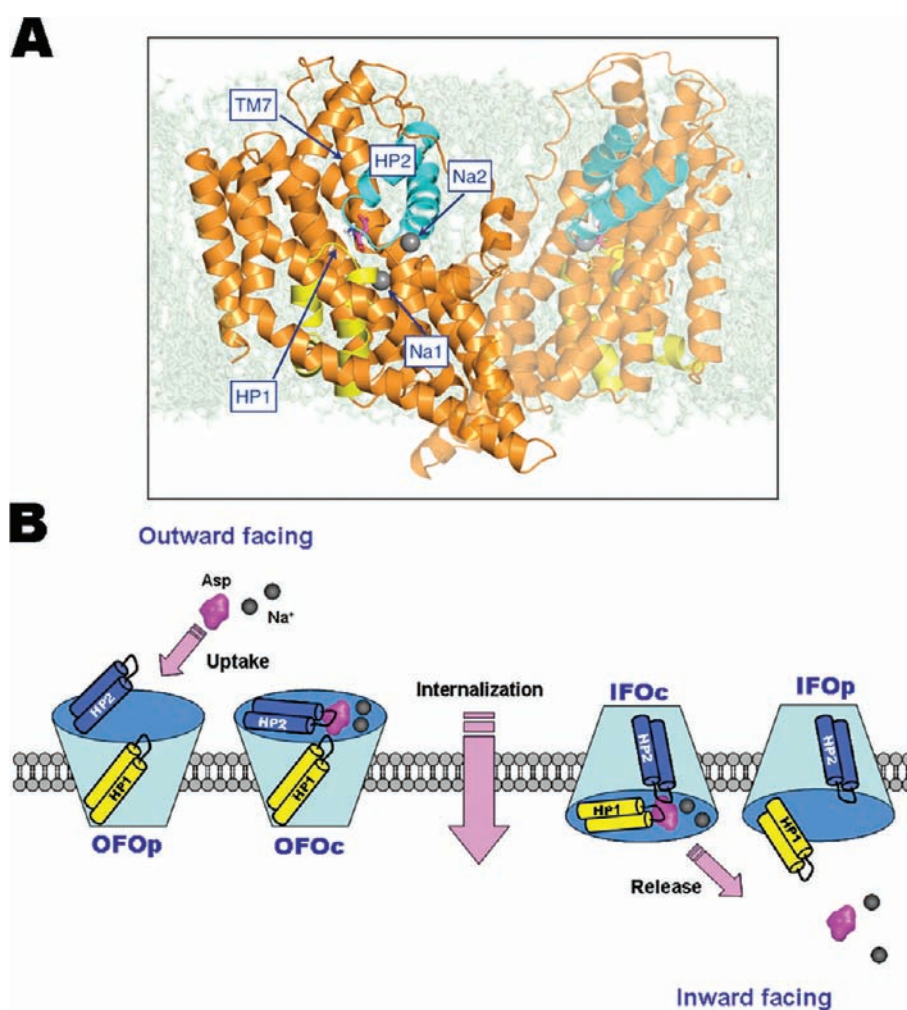
Figure 1. (A) Cartoon representation of the Glt_{Ph} transporter embedded in the membrane. The phospholypidic bilayer and the protein are represented as transparent green sticks and orange ribbons, respectively. The Asp is colored magenta, HP1 and HP2 are colored yellow and cyan, respectively, and the sodium ions are represented as gray spheres. The figure shows the perspective view from the third monomer, which is not displayed for clarity. (B) Schematic illustration of the conformational states of a Glt_{Ph} monomer representing the minimal functional unit of the transporter.

inward facing occluded (IFOc) where the Glu binding site is exposed toward the cytoplasm and HP1 is in the closed state; (iv) inward facing open (IFOp), with HP1 in the open state (Figure 1B). On the basis of this structural information, it has been hypothesized that the transporter passes from the OFOp state, competent for the substrate uptake from the extracellular environment, to the IFOp state, responsible for the substrate release in the intracellular environment. Very recently, Jiang et al.[7] confirmed that a stepwise transition of each of the three subunits is the most probable mechanism to enable the alternating access of the transporter. This mechanism is conserved among the sodium-dependent secondary transporters, such as the Na^+/H^+ antiporter (NhaA) and the leucine transporter (LeuT). On the basis of a symmetry relationship between the outward and the inward conformations of Glt_{Ph}, Crisman et al.[8] proposed that IFOc and IFOp can be obtained from OFOp and OFOc. Successively, Reyes et al.[6] confirmed in part the validity of Crisman's model by solving the structure of IFOc complexed with Asp, the lower homologue of Glu, while the IFOp conformation has not been yet experimentally determined.

Molecular dynamics (MD) studies have been carried out both on Glt_{Ph} and on homology models of human EAAT; however,

being mostly based on standard MD, they were able to explore only a limited time scale. These studies evidenced mobility of HP1 and HP2 in the outward and inward conformations and on the binding route of Glu to OFOp.[9,10] The only attempt to use enhanced sampling has been conducted on a structure of IFOc that later was proven to be not optimal.[11] Here, we lift the time issue by using a number of advanced sampling methods developed in our group[12] to study the four different conformations and the role of ligands (Asp and sodium ions), obtaining a comprehensive quantitative and qualitative description of the sequence of events that lead to substrate internalization. Many aspects previously described in experimental and theoretical studies are confirmed, while new important features are revealed here for the first time.

In particular, we were able to describe the complete opening mechanism in the outward states where a large scale motion of HP2 allows the substrate uptake. Mutatis mutandis, a similar role was played by HP1 in the inward release mechanism. We also investigated the crucial role played by Na^+ ions during the internalization process. Finally, the entire process was then quantitatively characterized and the free energy associated to each single event computationally calculated. The molecular

features involved in the protein conformational changes and the key interactions engaged by the ions and the substrate with the transporter are discussed in detail.

■ RESULTS AND DISCUSSION

The Model System. Our study was performed on a single monomer immersed in water. Since it is well-known that replacing both membrane and the other monomers with water is a rather harsh approximation, we added a small constraining potential on part of the monomer to ensure the same mechanical properties of the trimer. We tested the validity of this procedure by comparing it to the entire trimeric structure immersed in a solvated lipid bilayer.

No sizable distortion of the secondary structure, nor large deviation from the initial structure, was observed (see Computational Methods and Supporting Information). In addition, a number of experiments, such as those carried out by Jiang et al.,[7] have demonstrated that each monomer acts independently and that the internalization process does not take place at the interface between monomers,[13−15] suggesting that our level of description could be considered adequate.

The substrate was Asp, as the transporter used in our calculations, Glt_{Ph}, shows a much greater affinity for Asp ($K_D = 0.002\,\mu M$) than for Glu ($K_D = 122\,\mu M$).[5] Two Na^+ binding sites, hereafter referred to as Na1 ($Asp405^{TM8}$, $Gly306^{TM7}$, $Asn310^{TM7}$, $Ser278^{HP1}$, $Asn401^{TM8}$) and Na2 ($Thr352^{HP2}$, $Ser349^{HP2}$, $Ile350^{HP2}$, $Thr308^{TM7}$, $Met311^{TM7}$), were experimentally identified by Tl^+-soaked Glt_{Ph}.[5] The existence of the Na1 site has been confirmed by mutagenesis experiments,[16] while Na2 is considered a low affinity binding site for Na^+, and its location is debated. Actually, because Na2 is formed by backbone oxygens of HP2 and TM7, it has been rather complicated to validate it by means of mutagenesis studies. Nevertheless, Ryan et al.[17] characterized functionally the ion stoichiometry for Glt_{Ph}, demonstrating that the transport mechanism is coupled with at least two sodium ions. Larsson et al.[18] estimated by computational studies that the Na1 is a high affinity binding site ($\Delta G = -12.5$ kcal/mol) while Na2 displays marginal but still favorable affinity for Na^+ ($\Delta G = -4.7$ kcal/mol). Some of our metadynamics simulations showed that Na^+ in the Na2 site is quite unstable, pointing to an overall low ion binding affinity at this site.

Moreover, experimental[19] and theoretical studies[10] have indicated the presence of a third sodium ion that might play a role in the transport mechanism. Unfortunately, despite the efforts, its exact position is still debated. In fact, MD simulations and mutagenesis experiments[20] identified a potential third Na^+ binding site close to the side chains of $Asp312^{TM7}$ and $Thr92^{TM3}$. Conversely, Larsson et al.[18] have proposed that a potential third site can be partially formed by the β-carboxylate group of Asp, also showing that this site can be only transitorily occupied by Na^+. The latter hypothesis is also in agreement with a previous investigation by Tao and Grewer[21] and with electrostatic mapping studies reported by Holley and Kavanaugh.[22] Finally, Rosental et al.[23] have very recently identified a new cation binding site close to the side chain of $Asp390^{TM8}$, hypothesizing the presence of a potential fourth sodium binding site. In light of this debated scenario, here we investigated substrate internalization, taking into account the effect of Na^+ bound at Na1 and Na2 sites.

Experimentally, the conformational changes for the glutamate translocation in EAAT can take place in about 0.3 ms,[24] and therefore they cannot be sampled by using standard MD, whose accessible time scale is of the order of a few microseconds. To overcome this limitation, enhanced sampling techniques need to be used. Here in particular, we used metadynamics that relies on the addition of an external history-dependent potential acting on a few degrees of freedom, also called collective variables (CVs). In this way, the dynamics is accelerated and the free energy landscape calculated, provided that the choice of CVs has been careful. The choice of CVs can be relatively simple in the case of ligand/protein interaction where the distance between ligand and binding pocket often suffices to increase the observation of the binding events[25] but becomes more challenging where it comes to describe complex concerted motions that might require substantial rearrangement of macromolecules. In this work, we used path collective variables (PCVs)[26] to describe the large transition from the open to the closed states of HP1 and HP2. Given a reference path, one CV represents the progress along the chosen path, while the other CV describes the distance from it. PCVs have proven their usefulness in sampling large scale motion in proteins in a variety of applications.[27−29] In this framework, PCVs were used to simulate the open-to-closed transition, and whenever the binding of the ligands was studied, two additional CVs, namely a distance and a torsion CV, were added (see Computational Methods).

In the following sections, we report the results from the simulations for the transporter in the different outward and inward conformations and with different sodium ion stoichiometry.

The Outward Conformation. We study here the OFOp-to-OFOc transition and its free energy landscapes as function of ions and substrate stoichiometries. Furthermore, to gain insight on the substrate/transporter interactions, we also study the Asp unbinding process.

OFOp-to-OFOc Transition. According to Huang and Tajkhorshid,[9] Asp can interact with the transporter only after the binding of the first sodium to the Na1 site.[5] This hypothesis is plausible because once Asp is bound to the protein, the Na1 site is no longer accessible for sodium binding. Moreover, it has also been reported[5,9] that the Asp binding induces the HP2 conformational motion that allows the creation of a pocket (Na2), where a second sodium ion can bind. This scenario prompted us to study four systems:

A. Glt_{Ph} in the apo form (no ligand).
B. Glt_{Ph} in complex with one Na^+ (Na1 site).
C. Glt_{Ph} in complex with one Na^+ (Na1 site) and Asp.
D. Glt_{Ph} in complex with two Na^+ (Na1 and Na2 site) and Asp.

All these metadynamics simulations were carried out using the PCVs as defined in Computational Methods. The free energy surfaces (FES) associated with the transition between OFOp and OFOc are shown in Figure 2.

A. Glt_{Ph} Apo. In the apo form, the transporter was found to fluctuate barrierless between OFOp and OFOc (Figure 2A). This is due to the high mobility of HP2 (see Figure 1). A similar flexibility was described in the standard MD simulations of Huang and Tajkhorshid.[9] During our simulations, the binding pocket was constantly filled by water molecules and only one interhairpin H-bond between $Ser276^{HP1}$ and $Gly354^{HP2}$ was present. When this interaction was broken, the solvent filled the binding site leading to a more open HP2 conformation. This flexibility of HP2 was possible due to the absence of Asp and ions which would otherwise hamper the hairpin motion. A similar motion of HP2, albeit at higher extent, was observed in a recent study by Jiang et al.[7] on EAAT1. In particular, the authors have

455

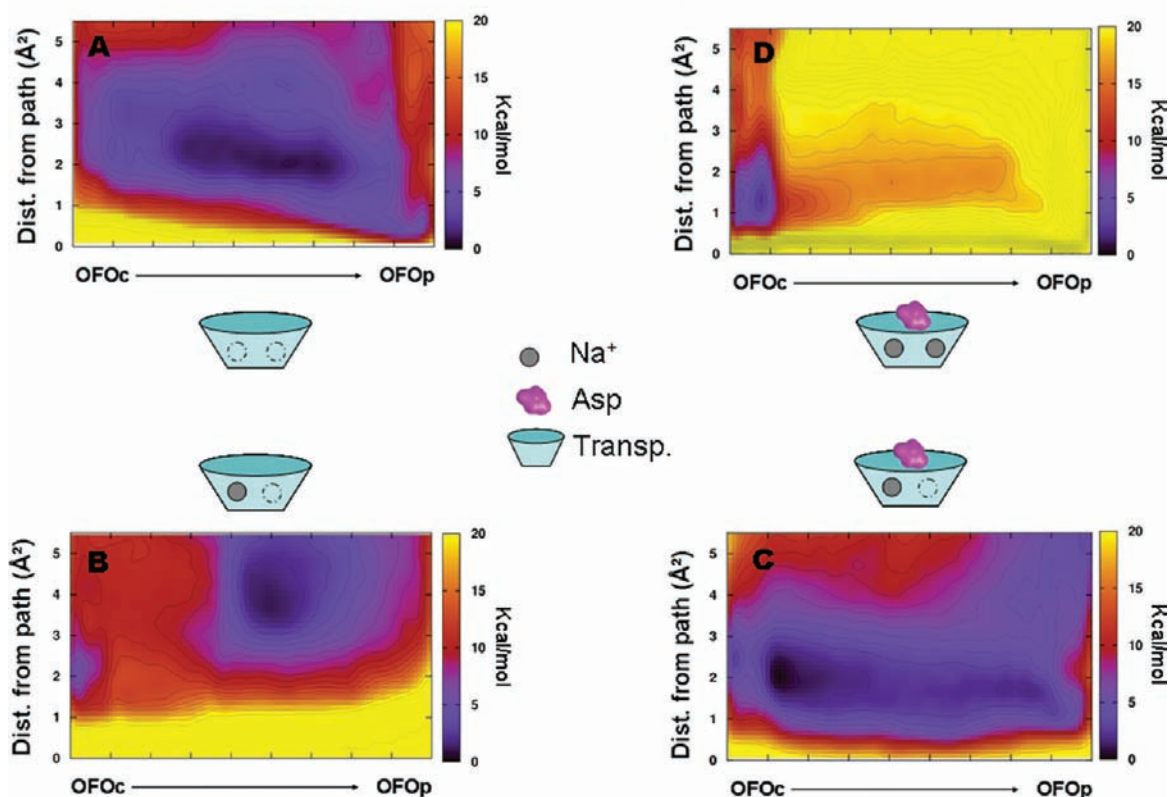dx.doi.org/10.1021/ja208485w | *J. Am. Chem. Soc.* 2012, 134, 453–463

External cycle

Figure 2. The FES at various stages of the Asp and Na$^+$ ion binding process. The FESs of the OFOc-to-OFOp transition using different stoichiometry of ligands bound to the transporter are shown: (A) transporter only, (B) transporter and the internal sodium ion (Na1 site), (C) monomer, one sodium ion (Na1 site), and Asp, (D) transporter, Asp, and both sodium ions (in Na1 and Na2 sites). The separation between contours is 1 kcal/mol. Each tick in the x axis represents one s units. For the sake of clarity, all the FESs are represented in the y range of 0−5.5 Å^2.

been able to stabilize the OFOp state by mutating some crucial residues such as Val449^{HP2} into cysteine. These results have suggested that HP2 could assume a fully and transitory open state. In line with these experiments, we found that OFOp was not stable in the apo form and that the structure reported in ref 4 is an effect of the complexation with bulky ligands such as TBOA.[5] Moreover, the open conformation assumed by HP2 is different from that found by Shrivastava et al.[30] In the conformation described by these authors, HP2 was only partially open and, within this framework, it can be considered an intermediate conformation (see following sections and Figure S1 in the Supporting Information). This underscores the advantage of adopting an enhanced sampling scheme to perform a more exhaustive sampling than standard MD can afford.

In our simulations, HP2 assumed several conformations between OFOc and OFOp that, being in equilibrium, were all equally possible. This suggests that the opening and the closing of the gate is a stochastic process, as also proposed in recent studies on Glt$_{Ph}$-related transporters.[31,32] In addition, our results confirm what has been observed through site-directed spin-labeling (DSDSL) electron paramagnetic resonance (EPR) spectroscopy, showing that in the Glt$_{Ph}$-unligated form, HP2 can assume a conformation similar to OFOc.[33]

B. Glt$_{Ph}$ + 1Na$^+$. The binding of one sodium ion at the Na1 site induced a significant change in the FES (compare Figure 2A and 2B). In fact, in this case the OFOc conformation was only

marginally stable, while a deep minimum appeared closer to the OFOp. In this basin, HP2 assumed an intermediate conformation between the OFOc and the OFOp states (Figure S1B, Supporting Information) away from reference path. One of the two α-helices forming the hairpin HP2, namely HP2a, assumed a conformation similar to that of the occluded state, while the second helix, HP2b, was more open, thus facilitating the uptake of Asp. A similar scenario has been depicted by Shrivastava et al.,[30] who found a reduced mobility of HP2a when compared to HP2b due to the close contacts formed by residues on HP2a and HP2tip (i.e., the domain connecting HP2a to HP2b), such as Gly354^{HP2} and Ala345^{HP2}, with residues on TM7, such as Ile309^{TM7} and Gln318^{TM7}. Our calculations confirm the existence of this intermediate conformation, as a result of the direct influence of the ions over the free energy landscape.

A comment is required here on the interpretation of our simulations in light of the recent experiments carried out by Focke et al.[33] and Claxton et al.[32] The former group[33] has observed, through DSDSL-EPR spectroscopy, that HP2 opens toward the TM4a, in good agreement with the outcomes of our calculations. These results prompted the authors to suggest that the binding of Na$^+$ stabilizes an open conformation of HP2, thus favoring the binding of the substrate. The latter group[32] carried out a FRET study using LeuT, suggesting a model whereby a cation-dependent conformational changes is able to create and stabilize the substrate-binding site. In good agreement with these
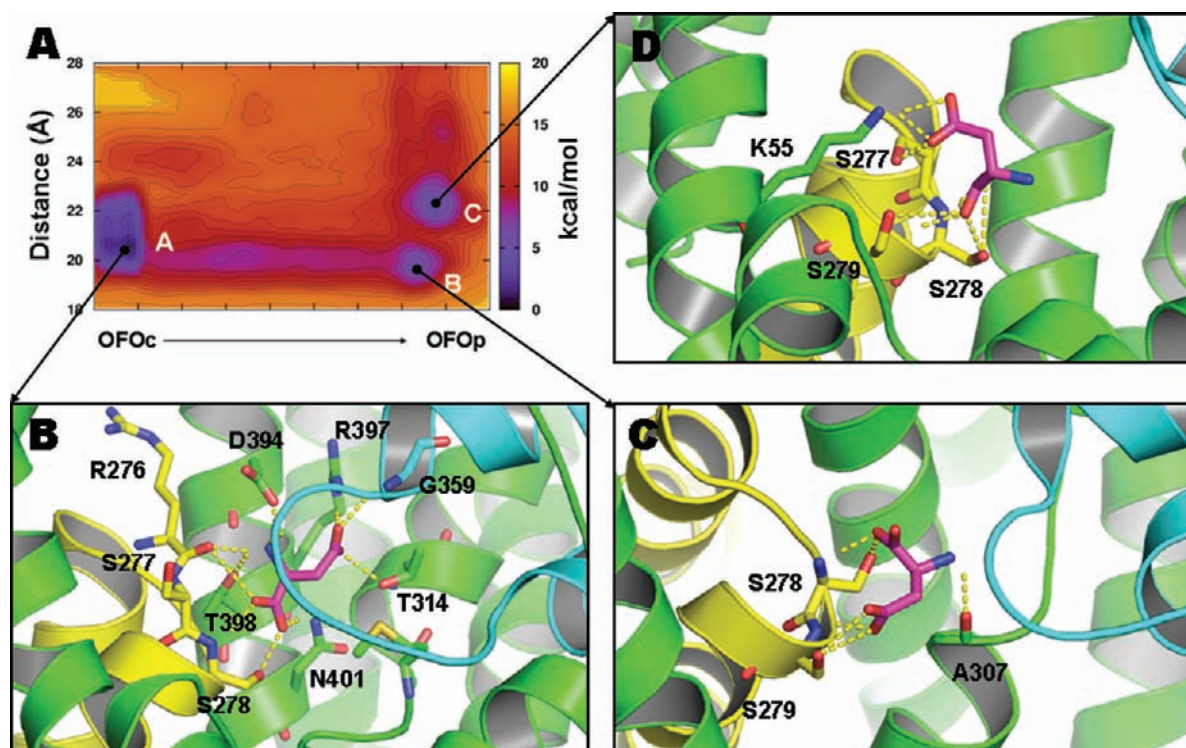
Figure 3. (A) The FES of the unbinding process of Asp as function of OFOc-to-OFOp transition (x axis) and the distance between Asp and the binding pocket (y axis). Isosurfaces are shown each kcal/mol. The molecular structures corresponding to the main energy minima A−C are highlighted in the insets B−D. The transporter is represented as ribbons and colored as follows: HP2 is cyan, HP1 is yellow, and the other transmembrane domains are green. The residues involved in the molecular interactions with Asp (magenta) are represented as sticks.

experimental studies, our results could explain the tight coupling between Na$^+$ binding and glutamate uptake, as also highlighted by Menaker et al.[34] Moreover, in line with this mechanistic hypothesis, the high physiological concentration of Na$^+$ can stabilize the OFOp state, favoring a prompt binding of the glutamate released in the glutamatergic synapses.

C. Glt$_{Ph}$ + 1Na$^+$ + Asp. At variance with what was seen previously, when Asp and one sodium ion were bound to Glt$_{Ph}$, the OFOc conformation was found to be more stable (of about 1.5 kcal/mol) than the OFOp one (Figure 2C). Nevertheless, this stability is weak and HP2 can easily move from the closed to the open state. The slight preference for the OFOc conformation is in line with the study of Huang and Tajkhorshid,[9] who reported that the combined binding of Na$^+$ and Asp is needed to stabilize HP2 in the closed form.

D. Glt$_{Ph}$ + 2Na$^+$ + Asp. Finally the second Na$^+$ was added at Na2 site. In Figure 2D, the deepest minimum corresponded to the crystallographic OFOc conformation. A comment on the functional role of the binding of the second sodium ion is in order here. In fact, our simulations point out that, while the first Na$^+$ along with Asp contributed to stabilize the closed form of HP2, the second Na$^+$ plays a fundamental role in locking Glt$_{Ph}$ in a conformation competent for Asp internalization. The depth of the energy basin corresponding to OFOc indicated that the binding of two Na$^+$ ions could strongly stabilize this state. However, our results cannot exclude the presence of a third Na$^+$, although this presence does not seem to have any functional role to achieve the OFOc state.

OFOc-to-OFOp Transition during the Asp Unbinding. To understand the structural features of the Asp uptake mechanism

from the extracellular region, we simulated the full unbinding of Asp from its pocket through metadynamics simulations. This was done using PCVs to sample the OFOc-to-OFOp transition as described before, plus two additional CVs. The first one was the distance defining the position of Asp relative to the protein, and the second was a torsion characterizing the different orientations assumed by the substrate (see also Computational Methods for details). In Figure 3A, the free energy landscape as a function of the OFOc-to-OFOp transition and the distance of Asp from the center of mass of selected residues of the protein is reported.

Three metastable states were found showing that Asp is able to bind different intermediate transporter conformations along the unbinding path. In particular, basin A corresponded to the deepest minimum with Asp in the crystallographic pose (OFOc), while basins B and C corresponded to two protein conformations close to the OFOp state, which occur with lower probability and can be thought of as invisible states.

In basin A, note all the interactions found by X-ray (Figure 3B), such as the H-bonds between one of the carboxylic groups of the ligand with Thr314^{TM7} and Gly359^{HP2} and the ionic bridge between the carboxyl and Arg397^{TM8}. Furthermore, H-bonds between the substrate and Ser277^{HP1}, Ser278^{HP1}, and Thr398^{TM8}, and an ionic bridge between the substrate and Asp394^{TM8}, were found, thus explaining the high energetic stability of the X-ray pose. In basins B and C, the ligand was still able to establish a number of interactions with the protein, despite the fact that it assumes a different orientation (Figure 3C,D). In particular, Asp formed a number of H-bonds with the serine-rich loop of the HP1 (i.e., Ser277-Ser278-Ser279). These serines are highly
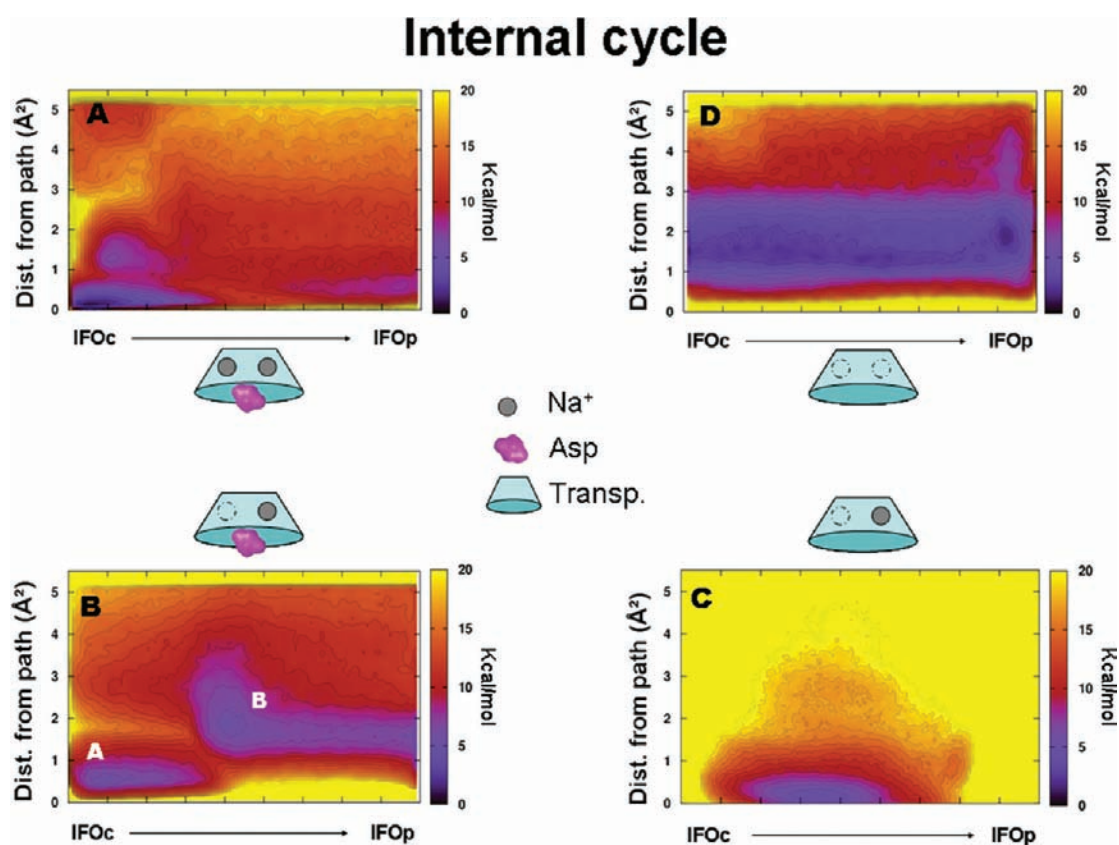
Figure 4. The FES at various stages of Asp and Na$^+$ ion release process. The FESs of IFOc-to-IFOp transition using different stoichiometry of ligands bound to the transporter are shown: (A) transporter, Asp, and two Na$^+$, (B) transporter, Asp, and one Na$^+$ at Na1, (C) transporter and one Na$^+$ at Na1, and (D) transporter without any ligand. The energy separation between contours is 1 kcal/mol. Each tick in the x axis represents one s unit. For the sake of clarity, all the FESs are represented in the y range of $0-5.5$ Å^2. Conformations at y values higher than 5 Å^2 were not explored using a constraint on the distance from path CV.

conserved in the mammalian transporter sequences, and their role in the uptake of the substrate was also supported by mutagenesis data.[35,36] In line with these experimental data and with the theoretical results of Shrivastava et al.,[30] our results suggest that the serine-rich loop is mainly involved in the Asp recognition process. In basin B, an additional H-bond between the α-amino group of Asp and the Ala307^{TM7} backbone is formed. This residue belongs to TM7 which is the domain connecting HP1 and HP2, thus reducing the flexibility of the hairpin motives. Moreover, at basin C an ionic bridge between Asp and Lys55^{TM2} was found. The role played by Lys55^{TM2} in the substrate transport mechanism is, for the first time, highlighted here, and the presence of this interaction assumes a greater relevance based on the fact that basic residues are well conserved at position 55 in the EAAT family.[37] Finally, when the ligand moves from basin C, it leaves the active site and points toward the extracellular region. During this last event, HP2 was found to be always in the open conformation.

To check the stability of the these poses, three unbiased MD simulations for a few nanoseconds were carried out, starting from the representative conformation of basins A, B, and C. In the case of A and C, the system was very stable with the ligand and the protein locked into conformations which supported the formation of favorable interactions. In the case of B, while the ligand maintained its binding conformation, HP2 fluctuated between the open and the closed state. We thus found a good correspondence

between the FES features and free MD results (Figure S2, Supporting Information).

Furthermore, with the aim of validating the results obtained on the monomer, we performed the same simulation on the trimeric system embedded in membrane. In particular we ran ~160 ns of simulations on the model system composed by 142,000 atoms. The FES (Figure S7, Supporting Information) was similar to that obtained using the monomer system (Figure 3) with the deepest basin representing the X-ray OFOc state (Figure 3B) and a second binding pocket corresponding to basin B (Figure 3C). This confirmed that the monomer provided a reliable model to study the functional mechanism of the transporter. This fact, together with the high computational cost of the simulations carried out on the trimeric system, prompted us to use the monomer in all the subsequent calculations.

The Inward Conformation. *IFOc-to-IFOp Transition.* To study the HP1 motion in the inward conformation, we applied the same protocol used to sample the HP2 motion in the outward conformation. Similarly to what we have done before, we used metadynamics together with PCVs to sample the open-to-closed transition. Contrary to OFOp, OFOc, and IFOc, the structure of IFOp has not yet been determined. However, recent experimental and theoretical studies point to the fact that IFOp can be determined on the basis of symmetry consideration.[6,8] We took the same point of view here, and we constructed the reference path for the IFOc-to-IFOp
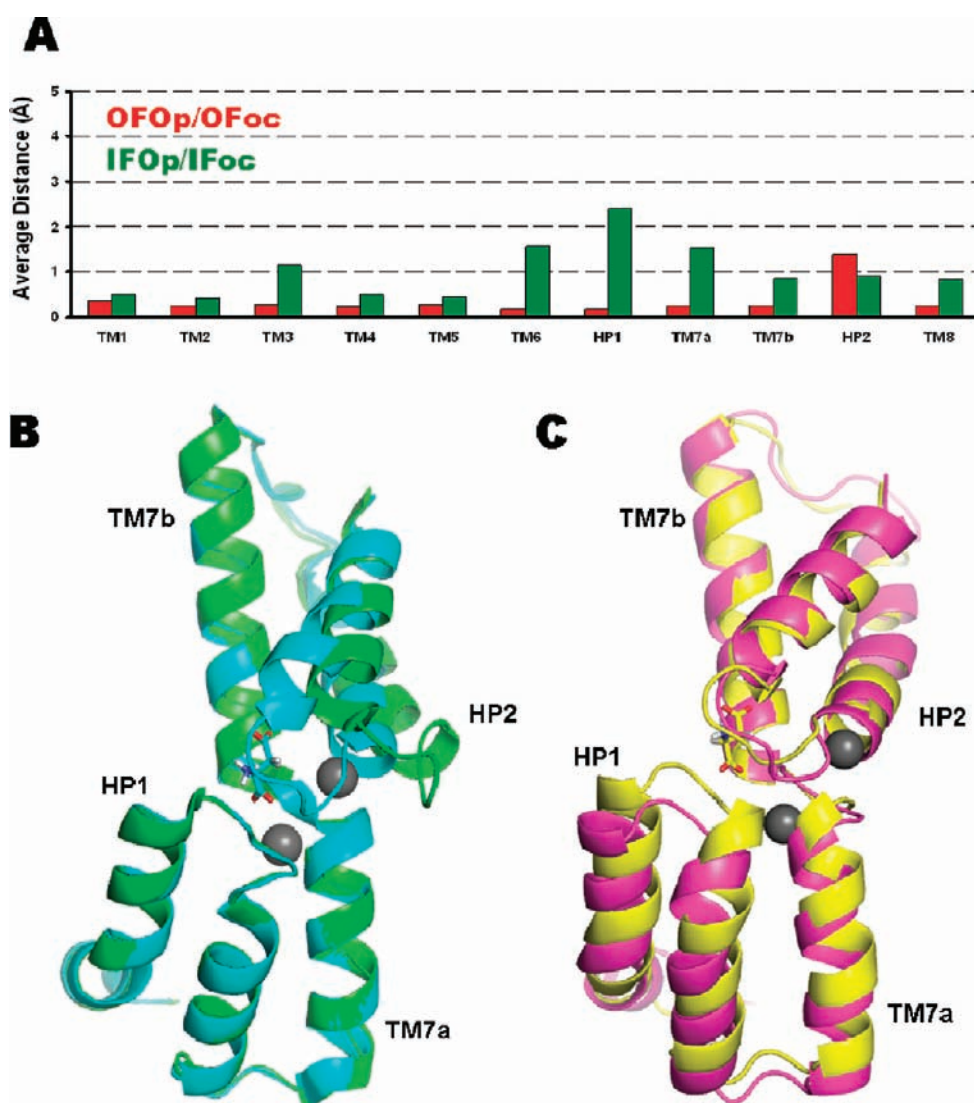
Figure 5. (A). Representation of the average distance in angstroms between Cα atoms belonging to the TM domains of OFOc with those of OFOp (red) and of IFOc with those of IFOp (green). For this calculation, the structures were aligned using TM1, TM2, TM4, and TM5, which maintain their position during the conformational changes. (B and C). Superimposition of the HP1, TM7, and HP2 domains of the outward facing (B) and inward facing (C) Glt$_{Ph}$ conformations. The secondary structures are represented as ribbons and colored depending on the Glt$_{Ph}$ conformational states. In particular, OFOp is green, OFOc is cyan, IFOc is yellow, and IFOp is magenta. Asp is represented as sticks, and the sodium ions, represented in their X-ray pose in the occluded states, are shown as gray spheres.

transition from that of the OFOc-to-OFOp transition. We expect this choice of initial path not to be crucial given the ability of PCVs to explore conformations different from the reference path.[25,26]

In the inward conformation, the chain of events described for the extracellular phase is expected to occur in the reverse order. In particular, the first event expected is the release of Na$^+$ from Na2 followed by the Asp unbinding. After these, the entrance of the intracellular water molecules to the binding cavity favors the release of the second sodium from Na1 into the intracellular region.

Therefore, similarly to the outward case, we performed four different runs on the transporter with different stoichiometry (Figures 4 and S3, Supporting Information). Having in mind the release process, we shall present our results in the reverse order relative to the outward case. We started then with the cavity fully occupied by two Na$^+$ and Asp. In this case, the system was found

locked in the IFOc conformation (Figure 4A), mirroring the case of the outward conformation reported in Figure 2D. In this state, the protein structure that resulted was similar to the crystallographic structure. The high stability of the closed state indicated that the presence of Na$^+$ in Na2 prevented local hydration of the binding pocket, thus increasing the stability of both Na$^+$ at Na1 and the bound substrate. As a consequence, the unbinding of Na$^+$ from Na2 should be an earlier event before the substrate internal release. This evidence is in good agreement with the study carried out by Zhao and Noskov using the LeuT transporter.[31]

After the release of the first Na$^+$ from Na2, the system increased the fluctuations around a structure which was similar to the IFOc (minimum A in Figure 4B). The FES in Figure 4B shows also the presence of another low energy basin (minimum B). Here, the transporter showed HP1 in a conformation intermediate between the closed and the open one, while HP2 was shifted
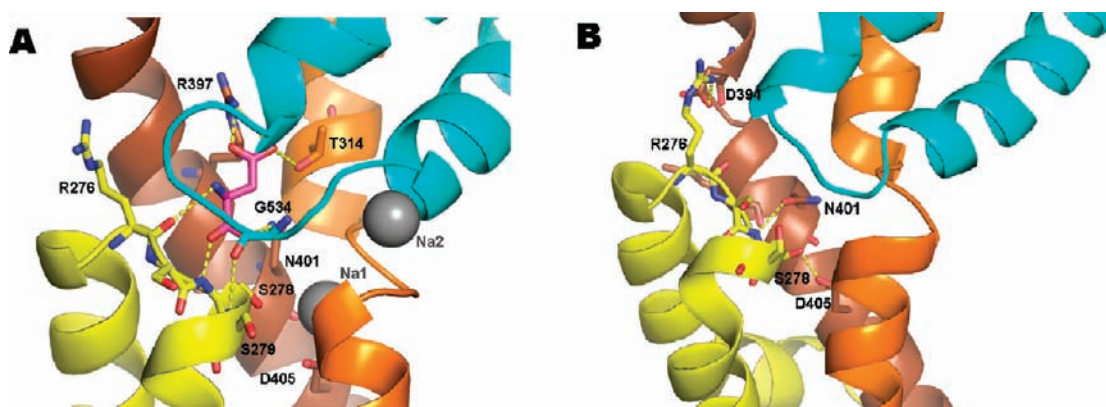
Figure 6. Schematic representation of the IFOc (A) and IFOp (B) conformations. The transporter is represented as ribbons and colored as follows: HP2 is cyan, HP1 is yellow, TM7 is orange, and TM8 is brown. The residues involved in the molecular interactions with Asp (magenta) are represented as sticks. Na$^+$ ions are shown as gray spheres.

toward the transmembrane domain TM2, where it formed a network of H-bonds with a number of residues belonging to the NMDGT motif, which is the most conserved portion of TM7 in the EAATs family.[4,37] The movement of HP2 was a consequence of the release of Na$^+$ from Na2. In fact, when it was bound to Na2, the sodium ion mediated a series of interactions between TM7 and HP2, providing a certain rigidity to the hairpin. Once Na$^+$ was released, these interactions were lost allowing a higher mobility of HP2 that moved toward TM2. In this new position, the HP2tip was no longer able to interact with the other hairpin, in particular with Ser279^{HP1}, while it engaged new contacts with residues such as Thr308^{TM7}, Asn310^{TM7}, and Met311^{TM7} (Figure S4, Supporting Information). The disruption of the interhairpin interactions allowed a major mobility of HP1 which was in a favorable condition for the subsequent substrate release. Moreover, in basin B, Asp engaged an H-bond with Ala358^{HP2} but lost its interaction with Val355^{HP2}, thus being more exposed to the solvent. That HP2 and HP1 are somewhat mobile have been observed also in the study of De Chancie et al.[38] We have revealed here the mechanistic details and the role of these hairpin motions in the release of the substrate. Our results are also in line with the study of Zhao and Noskov,[31] who have shown that, in case of the LeuT transporter, the release of Na$^+$ from Na2 triggers the release of Asp and Na$^+$ from Na1.

Once Asp was released, the hairpin flexibility increased. This was evident in the case of HP1, which assumes a number of conformations intermediate between IFOc and IFOp (Figure 4C). In particular, comparing these conformations with the crystallographic IFOc structure, one might note that HP1 was more opened toward the intracellular environment of about 2.0 Å, calculated using the distance between the Cα atoms of Arg276^{HP1} from Met390^{TM8} and Ser279^{HP1} from Thr308^{TM7}.

Finally, when Na$^+$ from Na1 was also removed (Figure 4D), the transporter fluctuated between the occluded (IFOc) and the open structure (IFOp), similarly to what happened in the open outward case (Figure 2A). This equilibrium would allow the conformational switch from IFOc to OFOc states in the absence of substrate, and the translocation across the membrane for the empty binding pocket, thus completing the whole transport cycle of the transporter. A similar mechanism has been very recently proposed by Focke et al.[33] Moreover, Zhao and Noskov[31] have observed for LeuT that the opening and the closing of the gate is a stochastic event, and that the equilibrium

distribution between the open and closed states is influenced by the presence of ions and substrate. We found that this is the case for the apo form of Glt$_{Ph}$, where IFOc and IFOp states could coexist and were equally possible.

Although the role of IFOp in the substrate release has been largely discussed in literature,[5−8] its structure has never been experimentally observed. The difficulties in determining the IFOp conformation are probably due to the fluxional nature of this state that exists only in the unligated form of Glt$_{Ph}$. Under this condition, the IFOc and the IFOp states are roughly equally probable. Therefore, so far, no experimental structure is available for this Glt$_{Ph}$ conformation. Here, the presence of a minimum, albeit shallow, led us to identify the IFOp structure corresponding to this minimum, which is described in detail in the next paragraph. Moreover, a comparison between the external and the internal conformational states is also deepened.

The IFOp Conformation. To disclose the main differences between the IFOc and the IFOp conformation, we have aligned both structures on the backbone atoms and measured the root mean square deviation (rmsd) of the heavy atoms for each residue (Figure 5A and 5D). In Figure 5A, one can observe that the region formed by TM6-HP1-TM7a (Gly238-Asn310) displayed the most relevant change with an average rmsd of 2.92 Å, much higher than the average value (1.4 Å).

A careful analysis of the molecular differences between IFOp and IFOc highlights that in the IFOc state the HP1 interacts with the TM7a and TM8 domains through a number of hydrophobic contacts and some polar interactions. In particular, the polar residues belonging to HP1 are exposed toward the intracellular region, while only the backbone atoms of the serine-rich loop interact with Asp (Figure 6A). The stability of the IFOc conformation was further increased by an additional H-bond between the backbone atoms of Ser279^{HP1} and Gly354^{HP2}.

At variance with IFOc, in the IFOp conformation, HP1 was stabilized by other favorable interactions. For instance, the Arg276^{HP1} side chain forms a salt bridge with Asp394^{TM8}, while Ser278^{HP1} H-bonds with the Gln401^{TM8} and Asp405^{TM8} side chains. The formation of the H-bond between Ser278^{HP1} and Asp405^{TM8} is probably at the basis of the partial misfolding of the HP1 helix, shown in Figure 6B. Furthermore, it is interesting to note that Gln401^{TM8} and Asp405^{TM8} are also involved in the binding of Asp and the sodium ion at Na1 in the IFOc state (Figure 6A).
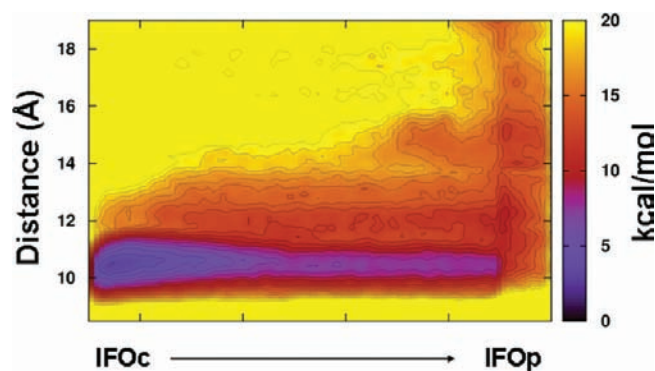
Figure 7. The FES of the unbinding process of Asp as a function of the IFOc-to-IFOp transition (x axis) and the distance between Asp and the binding pocket (y axis). Isosurfaces are shown each kcal/mol.

It is also interesting to compare the conformational changes that occur during the IFOc-to-IFOp transition with those of the OFOp-to-OFOc transition. Although some differences arise, the protein motion, that involves HP2 in outward facing conformation and HP1 in inward facing conformation, justifies a symmetry relationship. In fact, while the OFOc-to-OFOp transition involves mostly HP2 (Figure 5B and 5C), in the IFOc-to-IFOp transition, the movement involves a wider part of the protein with HP1 slightly shifted away from the binding site (Figure 5A and 5D). This highlights the fact that the symmetry between inward facing and outward facing conformations has a dynamical and functional meaning, in which different but structurally similar elements exchange their respective roles.

IFOc-to-IFOp Transition during Asp Unbinding. In the IFOc-to-IFOp transition, the sodium ion at Na2 was released while the other sodium ion at Na1 and Asp remained at their places. To better understand the process of Asp release into the intracellular milieu, we carried out a metadynamics simulations of Asp unbinding by using a setup identical to that adopted for the outward facing case. At variance with the Asp unbinding in the OFOc state (Figure 3), here we could observe only one minimum (Figure 7). This basin corresponded to the X-ray structure of the transporter with HP1 in the occluded state (Figure 6A). In particular, the FES showed that Asp was optimally located in the binding cleft (distance CV around 10 Å), engaging in a number of favorable interactions with the protein such as the polar contacts with Arg276[HP1], Ser278[HP1], Arg397[TM8], Thr314[TM7], and Gln401[TM8]. Once the ligand left the active site, it did not engage any relevant interactions with the protein, and no metastable states were detected. In fact, only some polar residues such as those of the serine-rich loop and Arg276[HP1] interacted transitorily with Asp during its internal release which appeared to be a diffusion process. Nevertheless, the free energy difference for the release was similar to the one detected for the outward facing case.

■ CONCLUSIONS

In this paper, we studied the aspartate uptake and internal release mechanism through the excitatory amino acid transporter from *Pyrococcus horikoshii* (Glt_{Ph}). This biochemical mechanism requires five major molecular events: (i) Asp binding to the transporter in the outward state and in the open conformation; (ii) conformational rearrangement of the transporter in the outward facing state from the open to the closed conformation; (iii) transition from the outward to the inward facing states; (iv) conformational rearrangement of the transporter in the inward

facing state from the closed to the open conformation; (v) Asp release in the extracellular environment. Here, four out of five steps of the overall mechanism have been investigated by means of all-atom computer simulations.

In the initial step, the transporter is in the outward facing state. This means that it is exposed at the extracellular level and can recognize and bind Asp, capturing it from the bulk of the solvent. This process is assisted by the binding of at least two Na$^+$ ions whose role has also been investigated. Using enhanced sampling techniques such as metadynamics, the events of interest are accelerated and can be simulated in affordable computational time. In so doing, we observed that Asp follows a specific path during its recognition process with the transporter engaging favorable contacts with a number of polar residues well-conserved across the EAAT protein family. Subsequently, the first major conformational change occurs and the transporter passes from the open to the closed conformation. During this closure mechanism, we found that while the first Na$^+$ contributes along with Asp to stabilize the closed form of HP2, the second Na$^+$ plays a fundamental role in locking Glt_{Ph} in a conformation competent for Asp internalization. The sequence of events for the Asp extracellular uptake can be summed up as follows: (i) the binding of the first Na$^+$ at Na1; (ii) the Asp binding; (iii) the binding of the second Na$^+$ at Na2.

After the last binding event, the transporter—Asp complex passes from the outward to the inward facing state as a consequence of a large conformational rearrangement. This event has not been studied here and represents a very challenging simulation that we have decided to undertake in the near future.

Once the transporter is in the inward state, a further conformational motion brings the transporter from the closed to the open conformation, allowing the release of Asp at the intracellular level. All the molecular details for this transition are provided and confirm that the symmetry relationship between the outward and the inward states holds not only structurally but also dynamically. As previously, we can sum the sequence of events also for the Asp intracellular release as follows: (i) the release of the first Na$^+$ from Na2; (ii) the Asp unbinding; (iii) the release of the second Na$^+$ from Na1.

Note that the IFOp conformation has not been solved so far. We identified this state as one of the transient conformational intermediates assumed by the transporter and reported its detailed structural description in the Supporting Information. Using metadynamics we were able to calculate the free energy profile associated with the simulated processes. This allowed the elucidation of the role played by the ligands, sodium ions, and Asp, during the major conformational changes of the transporter. Figure 8 shows an artistic representation of the potential energy associated with the steps here investigated.

Our study represents a comprehensive report on the entire mechanism of reuptake of the excitatory neurotransmitters (Glu or Asp) that can shed some light on the physiology of this complex machinery. Moreover, the design of new ligands of pharmacological relevance in diseases such as Alzheimer's and Parkinson's could strongly benefit from the present study on the detailed interaction occurring in the uptake and release process. In fact, the whole description of the OFOp—OFOc and IFOc—IFOp transition provides new molecular targets for the development of innovative ligands able to block the transport of excitatory amino acids at different levels under pathologic conditions.
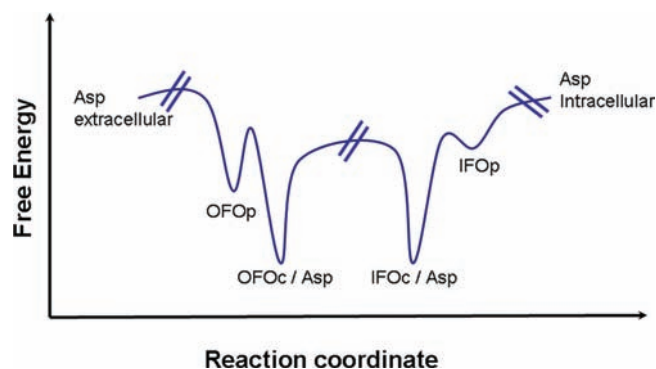
Figure 8. Artist's impression of the suggested potential energy surface of the Glt$_{Ph}$.

■ COMPUTATIONAL METHODS

The full computational procedure used to set up the systems is reported in detail in the Supporting Information. Here we draw attention to the metadynamics protocol.

Well-Tempered Metadynamics. To enhance the sampling of the configurational space and to reconstruct the free energy surface (FES) as a function of some order parameters, namely CVs (see below), metadynamics simulations were carried out.[39] Briefly, metadynamics consists of an adaptive scheme where Gaussian-shaped repulsive potentials are deposited along the simulation in the space of the chosen collective variables. This discourages the system from sampling the configurations already visited and eventually it serves as an estimator of the FES.[40] Here, in particular, we employed the well-tempered variant[41] in which the height of the repulsive potential introduced is decreased with the amount of bias already deposited, providing a free energy estimation that reads:

$$F(s,t) = -\frac{T + \Delta T}{T} V(s,t) \tag{1}$$

where $V(s,t)$ is the bias potential added to the system and T is the temperature of the simulation. ΔT is called "bias factor" and represents the virtual temperature along the used degrees of freedom (CVs), and $F(s,t)$ is the free energy estimate obtained from the bias $V(s,t)$.

Thanks to this new formalism, the time needed for barrier crossing is lowered, facilitating the exploration in the CVs space by tuning ΔT and, at the same time, obtaining a converging free energy estimate. Moreover, by using a finite value of ΔT, the exploration of the FES can be limited to the low free energy regions within an energy range of the order $T + \Delta T$.

In our set of simulations, Gaussian potentials with deposit rate of 1.1 kcal/mol per picosecond were initially deposited and gradually decreased on the basis of the adaptive bias with a ΔT of 3000 K.

Metadynamics Simulations with PCVs. The crystal structures of OFOc and OFOp suggest that the transition between the two states is highly cooperative and involves a number of degrees of freedom. In this kind of motion, the use of a distance or a torsion CV might be insufficient in reproducing the transition and in calculating the free energy. For these reasons, the path collective variables (PCVs) approach was introduced and in a few years they were successfully exploited in a number of applications.[24−28] In this scheme, two functions are introduced which characterize the position of a point in configurational space R relative to a preassigned path in terms of progress along the path $s(R)$ and distance from it $z(R)$. In the present case, the preassigned path coincides with the interpolation (see below) from OFOp/OFOc transition.

The variables $s(R)$ and $z(R)$ can be written as:

$$s(R) = \frac{\sum_{i=1}^{P}(i)e^{-\lambda[(R-R(i)]^2}}{\sum_{i=1}^{P}e^{-\lambda[R-R(i)]^2}} \tag{2}$$

$$z(R) = -\frac{1}{\lambda}ln\left(\sum_{i=1}^{P}e^{-\lambda[R-R(i)]^2}\right) \tag{3}$$

where i is a discrete index ranging from 1 to P and where P is the number of conformations in the "template" path obtained via interpolation. In the present case, $[R - R(i)]^2$ is calculated as the mean square displacement after optimal alignment by using Kearsley's algorithm.[42] The choice of the coordinates of atoms to be included in the path is far from trivial because a wrong choice can turn into a loss of performance and additional noise that may hamper the results of the calculations.

OFOc-to-OFOp Path. In this case we used the Cα of the residues belonging to HP1 (Thr275 to Ser 279) and to HP2 (Leu339 to Val367), that represent the minimal set of atoms necessary to simulate the OFOc-to-OFOp transition. This choice was found to be appropriate because the calculated FESs were well reproducible. The initial path was obtained through a curvilinear interpolation from the OFOp to the OFOc conformation using the morphing utility (g_morph) of the GROMACS suite.[43] The final path consists of 10 frames. We verified that the obtained set of configurations was equally spaced in the adopted mean square displacement metrics, and the value of λ was chosen to be comparable to the inverse of the mean square displacement between successive frames.[43] Because the path obtained from the morphing procedure could be rather unphysical, a preliminary metadynamics run was performed so as to find the closest physical representative path of our guess transition. Finally, from the resulting trajectory a new set of more reliable, physically relevant and equally spaced frames was extracted and used in eqs 2 and 3 (Figure S5, Supporting Information).

The average distance between adjacent frames was 1.31 Å, thus requiring to set $\lambda = 5.36$ Å^{-2} in eqs 2 and 3. The hill width was chosen to be 0.2 for s and 0.2 Å^2 for z according to their fluctuation in standard MD. The path obtained was considered reliable because using this in metadynamics simulations, the OFOc-to-OFOp transition is reproduced and the lowest free energy paths are found at low distances from the reference path. This is proof that the reference path was representative of the transition (see Figure 2A) and was able to provide a reliable free energy landscape.

IFOc-to-IFOp Path. To build the opening path from IFOc-to-IFOp states, due to the symmetry relationship of HP1 and HP2,[5,8] it was considered plausible that the HP1 conformation in the IFOp state was not very different from that of HP2 in the OFOp conformation. Consequently, we adapted the optimized path for the OFOc-to-OFOp transition into a suitable path for the IFOc-to-IFOp transition. Because the role of the hairpins should be reversed in the IF respect to the OF, the alignment was performed by structurally superimposing the Cα of HP1 in the IFOp with the Cα of HP2 of the OFOp and the same was performed for the HP2 domain with respect to HP1. In so doing, we built an initial IFOc-to-IFOp path that was further refined using metadynamics simulation with PCVs (see the protocol adopted in the previous calculations). The average distance between adjacent frames finally obtained was 0.4 Å, thus requiring $\lambda = 14.66$ Å^{-2} in eqs 2 and 3. The hill width was chosen to be 0.1 for s and 0.1 Å^2 for z as suggested by the fluctuation of these CVs in standard MD. The obtained path was considered reliable according the above-mentioned criteria and was used for metadynamics on the IF systems with different stoichiometry of ligands (Figure 4) and for the simulation of the Asp intracellular release (Figure 7).

462

dx.doi.org/10.1021/ja208485w |*J. Am. Chem. Soc.* 2012, 134, 453–463

Metadynamics Simulations of Asp Uptake/Release. In addition to PCVs, we used two further CVs, a distance and a torsion CV, to sample the Asp translocation from the extracellular to the intracellular environment and to find the transporter residues engaged during this process. In detail, we considered the distance between the center of mass of the ligand and of a selected group of $C\alpha$ atoms of the transporter, and a torsion angle that describes the different orientation assumed by Asp in the binding pocket (see Supporting Information for details). This kind of CV has been already used with success in other complex docking studies.[25,28] During the metadynamics simulations, the bias was added simultaneously on s, distance, and torsion angle CVs, resulting in the FESs reported in Figures 3 and 7. Here, it is important to mention that in these figures the FESs are represented as function of s and the distance CV while the torsion CV is integrated but not shown. Moreover, note that the distance CV value, that describes Asp in the bound states to OFOc and IFOc, is not zero. Instead, when bound, it assumes a value of 20 Å and 10 Å for the complex in the OFOc and IFOc conformations, respectively. The figures were rendered using the PyMOL software[44] while graphs were generated using gnuplot.[45]

■ ASSOCIATED CONTENT

Ⓢ **Supporting Information.** Details related to computational methods and additional figures. This material is available free of charge via the Internet at http://pubs.acs.org.

■ AUTHOR INFORMATION

Corresponding Author
andrea.cavalli@unibo.it; parrinello@phys.chem.ethz.ch

■ ACKNOWLEDGMENT

■ REFERENCES

(1) Cavallero, A.; Marte, A.; Fedele, E. *J. Neurochem.* **2009**, *110*, 924–934 and cited references.

(2) (a) Bergles, D. E.; Diamond, J. S.; Jahr, C. E. *Curr. Opin. Neurobiol.* **1999**, *9*, 293–298. (b) Jiang, J.; Amara, S. G. *Neuropharmacology* **2011**, *60*, 172–181. (c) Krishnamurthy, H.; Piscitelli, C. L.; Gouaux, E. *Nature* **2009**, *459*, 347–355.

(3) Maragakis, N. J.; Rothstein, J. D. *Neurobiol. Dis.* **2004**, *15*, 461–473.

(4) Yernool, D.; Boudker, O.; Jin, Y.; Gouax, E. *Nature* **2004**, *431*, 811–818.

(5) Boudker, O.; Ryan, R. M.; Yernool, D.; Shimamoto, K.; Gouaux, E. *Nature* **2007**, *445*, 387–393.

(6) Reyes, N.; Ginter, C.; Boudker, O. *Nature* **2009**, *462*, 880–885.

(7) Jiang, J.; Shrivastava, I. H.; Watts, S. D.; Bahar, I.; Amara, S. G. *Proc. Natl. Acad. Sci. U.S.A.* **2011**, *108*, 15141–15146.

(8) Crisman, T. J.; Qu, S.; Kanner, B. I.; Forrest, L. *Proc. Natl. Acad. Sci. U.S.A.* **2009**, *106*, 20752–20757.

(9) Huang, Z.; Tajkhorshid, E. *Biophys. J.* **2008**, *95*, 2292–2300.

(10) Huang, Z.; Tajkhorshid, E. *Biophys. J.* **2010**, *99*, 1416–1425.

(11) Gu, Y.; Shrivastava, I. H.; Amara, S. G.; Bahar, I. *Proc. Natl. Acad. Sci. U.S.A.* **2009**, *106*, 2589–2594.

(12) Parrinello, M. In *Physical Biology From Atoms to Medicine*; Zewail, A. H., Ed.; Imperial College Press: London, 2008; pp 247–265.

(13) Grewer, C.; Balani, P.; Weidenfeller, C.; Bartusel, T.; Tao, Z.; Rauen, T. *Biochemistry* **2005**, *46*, 11913–11923.

(14) Koch, H. P.; Larsson, H. P. *J. Neurosci.* **2005**, *25*, 1730–1736.

(15) Koch, H. P.; Brawn, R. L.; Larsson, H. P. *J. Neurosci.* **2007**, *27*, 2943–2947.

(16) Teichman, S.; Qu, S.; Kanner, B. I. *Proc. Natl. Acad. Sci. U.S.A.* **2009**, *106*, 14297–14302.

(17) Ryan, R. M.; Compton, E. L. R.; Mindell, J. A. *J. Biol. Chem.* **2009**, *26*, 17540–17548.

(18) Larsson, H. P.; Wang, X.; Lev, B.; Baconguis, I.; Caplan, D. A.; Vyleta, N. P.; Koch, H. P.; Diez-Sampedro, A.; Noskov, S. Y. *Proc. Natl. Acad. Sci. U.S.A.* **2010**, *107*, 13912–13917.

(19) Groeneveld, M.; Slotboom, D. *Biochemistry* **2010**, *49*, 3511–3513.

(20) Tao, A.; Rosental, N.; Kanner, B. I.; Gameiro, A.; Mwaura, J.; Grewer, C. *J. Biol. Chem.* **2010**, *285*, 17725–1733.

(21) Tao, Z.; Grewer, C. *J. Gen. Physiol.* **2007**, *129*, 331–344.

(22) Holley, D. C.; Kavanaugh, M. P. *Philos. Trans. R. Soc. Lond., B* **2009**, *364*, 155–161.

(23) Rosental, N.; Gameiro, A.; Grewer, C.; Kanner, B. I. *J. Biol. Chem.* **2011**, *286*, 41381–41390.

(24) Mim, C.; Tao, Z.; Grewer, C. *Biochemistry* **2007**, *44*, 9007–9018.

(25) Gervasio, F. L.; Laio, A.; Parrinello, M. *J. Am. Chem. Soc.* **2005**, *127*, 2600–2607.

(26) Branduardi, D.; Gervasio, F. L.; Parrinello, M. *J. Chem. Phys.* **2007**, *126*, 0540103.

(27) Berteotti, A.; Cavalli, A.; Branduardi, D.; Gervasio, F. L.; Recanatini, M.; Parrinello, M. *J. Am. Chem. Soc.* **2009**, *131*, 244–250.

(28) Limongelli, V.; Bonomi, M.; Marinelli, L.; Gervasio, F. L.; Cavalli, A.; Novellino, E.; Parrinello, M. *Proc. Natl. Acad. Sci. U.S.A.* **2010**, *107*, 5411–5416.

(29) Pfaendtner, J.; Branduardi, D.; Parrinello, M.; Pollard, T. D.; Voth, G. A. *Proc. Natl. Acad. Sci. U.S.A.* **2009**, *106*, 12723–12728.

(30) Shrivastava, I. H.; Jiang, J.; Amara, S. G.; Bahar, I. *J. Biol. Chem.* **2008**, *283*, 28680–28690.

(31) Zhao, C.; Noskov, S. Y. *Biochemistry* **2011**, *50*, 1848–1856.

(32) Claxton, D. P.; Quick, M.; Shi, L.; Delmondes de Carvalho, F.; Weinstein, H.; Javitch, J.; Mchaourab, H. S. *Nat. Struct. Biol.* **2010**, *17*, 822–830.

(33) Focke, P. J.; Moenne-Loccoz, P.; Larsson, H. P. *J. Neurosci.* **2011**, *31*, 6255–6262.

(34) Menaker, D.; Bendahan, A.; Kanner, B. I. *J. Neurochem.* **2006**, *99*, 20–28.

(35) Seal, R. P.; Leighton, B. H.; Amara, S. G. *Neuron* **2000**, *25*, 695–706.

(36) Slotboom, D. J.; Sobczak, I.; Konings, W. N.; Lolkema, J. S. *Proc. Natl. Acad. Sci. U.S.A.* **1999**, *96*, 14282–14287.

(37) Ryan, R. M.; Mitrovic, A. D.; Vanderberg, R. J. *J. Biol. Chem.* **2004**, *20*, 20742–20751.

(38) DeChancie, J.; Shrivastava, I. H.; Bahar, I. *Mol. BioSyst.* **2011**, *7*, 832–842.

(39) Laio, A.; Parrinello, M. *Proc. Natl. Acad. Sci. U.S.A.* **2002**, *99*, 12562–12566.

(40) Bussi, G.; Laio, A.; Parrinello, M. *Phys. Rev. Lett.* **2006**, *96*, 090601.

(41) Barducci, A.; Bussi, G.; Parrinello, M. *Phys. Rev. Lett.* **2008**, *100*, 020603.

(42) Kearsley, S. K. *Acta Crystallogr., Sect. A: Found. Crystallogr.* **1989**, *45*, 628–635.

(43) Hess, B.; Kutzner, C.; van der Spoel, D.; Lindahl, E. *J. Chem. Theory Comput.* **2008**, *4*, 435–447.

(44) DeLano, W. L. *The PyMOL Molecular Graphics System*, Schrödinger, LLC, http://www.pymol.org

(45) Williams, T.; Kelley, C. *GNUPLOT: An Interactive Plotting Program*, 1993